IEEE Access
Multidisciplinary ⋮ Rapid Review ⋮ Open Access Journal

Received 6 June 2022, accepted 23 June 2022, date of publication 27 June 2022, date of current version 1 July 2022.

Digital Object Identifier 10.1109/ACCESS.2022.3186713

Design of Model-Free Speed Regulation System for Permanent Magnet Synchronous Linear Motor Based on Adaptive Observer

ZHENG LI[1,2], (Member, IEEE), ZIHAO ZHANG[1], SHENGDI FENG[1], JINSONG WANG[1], XIAOQIANG GUO[2], (Senior Member, IEEE), AND HEXU SUN[1], (Senior Member, IEEE)

[1]School of Electrical Engineering, Hebei University of Science and Technology, Shijiazhuang, Hebei 050018, China
[2]School of Electrical Engineering, Yanshan University, Qinhuangdao, Hebei 066004, China

Corresponding authors: Zheng Li (Lizheng@hebust.edu.cn) and Hexu Sun (sunhxhb@outlook.com)

This work was supported in part by the National Natural Science Foundation of China under Grant 51877070, Grant U20A20198, and Grant 51577048; in part by the Natural Science Foundation of Hebei Province of China under Grant E2021208008; in part by the Talent Engineering Training Support Project of Hebei Province under Grant A201905008; and in part by the National Engineering Laboratory of Energy-saving Motor and Control Technique, Anhui University, under Grant KFKT201901.

ABSTRACT To simplify the system structure of permanent magnet synchronous linear motor (PMSLM), optimize the kinematic performance of the control system, and further improve the speed tracking accuracy of PMSLM, a model-free speed regulation system design of PMSLM based on the adaptive observer is proposed. Aiming at the control instability problem caused by the parameter uncertainty of PI control in PMSLM, a model-free speed controller (MFC) based on the ultra-local model is proposed, which has strong robustness to the uncertainty of motor parameters. Meanwhile, the actual model of PMSLM is used to build the reference model of the adaptive observer, and the adjustable model is designed with the current equation of PMSLM, to identify the speed of PMSLM. The design not only reduces the dependence of the speed controller on the motor parameters, but also simplifies the complexity and cost of the control system, and improves the control performance and anti-interference ability of the control system. The MFC and the observer based on the model reference adaptive system (MRAS) are built by simulation software and applied to the PMSLM system to verify the superiority of the designed control system. Compared with PI controller, sliding mode controller (SMC), and sliding mode observer (SMO), this control method not only simplifies the control system in structure, but also improves the accuracy of PMSLM tracking speed, improves the dynamic response performance of PMSM control system, and optimizes the control ability of the control system.

INDEX TERMS Permanent magnet synchronous linear motor, model-free control, ultra-local model, adaptive observe.

I. INTRODUCTION

With the rapid development of modern industrial technology, society's control accuracy and manufacturing requirements for the manufacturing industry are increasing day by day. Permanent magnet synchronous linear motors have broad development prospects because they provide linear power, high precision, and fast response without any mechanical interface. It has great potential for development in the fields of industrial robots and CNC machine tools [1], [2]. Compared with traditional rotary motor systems, permanent magnet linear motors have no friction and elastic deformation during mechanical transmission, so they have been widely used in industrial fields that require high control accuracy [3], It can not only improve the control precision of the system but also shorten the reaction time of the feed system [4]. However, PMSLM has a saturation effect and side effect, which makes it difficult to control the system with high precision [5].

The associate editor coordinating the review of this manuscript and approving it for publication was Okyay Kaynak.

Strong robustness and high precision have become the development trend of the speed loop in the PMSLM control system [6]. At present, the main control strategy is predictive control [7], [8], Model-free control [9]–[11], PI control, and adaptive control [12]. Literature [13] applied predictive control to the PMSLM control system to improve the speed controller, ensure the strong robustness of the linear motor system, and reduce the speed fluctuation. Many control methods have been proposed, such as active disturbance rejection control (ADRC), model-free adaptive control (MFAC), and MFC. ADRC has a clear control idea and provides a systematic solution for nonlinear systems with uncertainties [14], [15]. However, because the multi-parameter optimization of ADRC is difficult to achieve, the optimal control of the system is not easy to achieve. MFAC estimates the pseudo partial derivative according to the input and output data of the controlled system, then establishes the equivalent dynamic linearization model, and then establishes MFAC [16], [17]. However, for systems with complex nonlinearity, MFAC based on compact form dynamic linearization cannot guarantee its performance. MFC only relies on the input and output data of the controlled system to establish the ultra-local model and its controller [18]. In the application based on DC motor, MFC is a good solution against load disturbance and parameter change [19]. SMC is less sensitive to the choice of control parameters than MFC, but SMC jitter is inevitable. At the same time, the comparative study of MFAC and MFC shows that both schemes perform well, but the parameters of MFC that need to be optimized are relatively few [20].

In the motor control system, sensorless technology is introduced to better reflect the control performance of the controller and make the feedback information of the control system to the controller fast and accurate. Compared with speed control technology with a speed sensor, sensorless technology can observe rotor flux and speed through designed observers. At present, commonly used observers include the Kalman filtering algorithm [21], model reference adaptive algorithm [22], and sliding mode observer algorithm [23], [24]. Among them, the sliding mode observer algorithm is simple in design and has a strong dynamic response-ability, but it may cause chattering of the system due to its attributes [25]. Kalman filtering algorithm can estimate the system state online and control the system in real-time, but the amount of calculation is too large and the system adjustment time is too long [26]. Model Reference Adaptive System Observer (MRAS) performs parameter identification of the motor through Adaptive rate, which improves the robustness of the System [27], [28].

In this paper, a model-free speed control strategy for PMSLM based on an adaptive observer is designed. Based on model-free control, a new model-free speed control method for PMSLM is proposed. Based on the ultra-local model, the model-free speed controller of the PMSLM control system is established, which solves the problem of control instability caused by the parameter uncertainty of traditional control methods, and has strong robustness. Meanwhile, the MRAS uses the actual model of the motor design, the adjustable model using the estimate of the current model to carry on the design, through the current difference between the reference model and adjustable model estimate motor speed, the design of the adaptive law in simplifying the structure of the system at the same time, improves the speed of the system tracking precision. Meanwhile, Popov hyperstability theory and Lyapunov stability theory are used to analyze the stability of MRAS. Finally, simulation software is used to verify the superiority of the proposed control strategy, and its feasibility and effectiveness are verified by simulation and experiment.

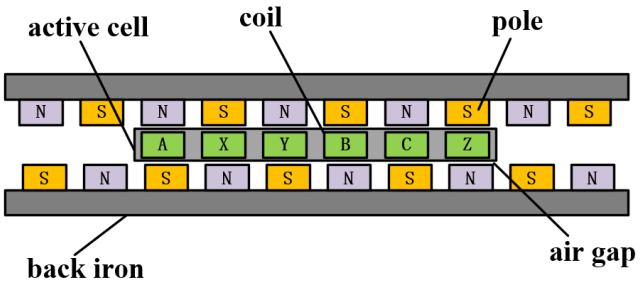

FIGURE 1. Structure diagram of PMSLM.

II. MATHEMATICAL MODEL OF PMSLM

The PMSLM selected in this design is a double-sided magnetic pole ironless PMSLM, and the basic structure is shown in Figure 1.

In the PMSLM system, the voltage equation on the stator in the rotating coordinate system can be expressed as:

$$\begin{cases} u_d = Ri_d + L_d \frac{d}{dt} i_d - \omega_c L_q i_q \\ u_q = Ri_q + L_q \frac{d}{dt} i_q + \omega_c (L_d i_d + \psi_f) \\ \omega_c = \frac{\pi \cdot v}{\tau} \end{cases} \tag{1}$$

in the above formula, R is the stator resistance in a linear motor; τ is the polar moment in a linear motor; v is the speed in the running process of the linear motor; u_d, u_q are the voltage components of the $d-q$ axis, respectively. i_d, i_q are the current components of the $d-q$ axis, respectively. L_d, L_q are the inductive components of the $d-q$ axis, respectively. ω_c is the angular velocity of the PMSLM; ψ_f is the permanent magnet flux of the linear motor.

The electromagnetic thrust equation of PMLSM is:

$$F_{em} = p_n \frac{3\pi}{2\tau} [\psi_f i_q + (L_d - L_q) i_d i_q] \tag{2}$$

in the above formula, F_{em} represents the thrust of the linear motor; p_n represents the polar logarithm of the linear motor.

The experimental object used in this paper is surface mount PMSLM, which satisfies $L_d = L_q = L$. Therefore, the thrust equation of the linear motor can be rewritten as:

$$F_{em} = p_n \cdot \frac{3\pi}{2\tau} \cdot \psi_f \cdot i_q \tag{3}$$

the mechanical motion equation of the PMSLM is:

$$m_e \cdot \frac{dv}{dt} = F_{em} - f - B_e \cdot v \tag{4}$$

in formula (4), m_e is the mass of the mover in the linear motor; B_e is viscous friction factor in the linear motor; f represents disturbance term in the linear motor control system. Formula (3) and formula (4) can be obtained simultaneously:

$$\frac{dv}{dt} = a_M \cdot i_q + b_M \cdot v + c_M \cdot f \tag{5}$$

in formula (5), $a_M = \frac{1}{m_e} p_n \cdot \frac{3\pi}{2\tau} \cdot \psi_f$; $b_M = -\frac{B_e}{m_e}$; $c_M = -\frac{1}{m_e}$

III. PMSLM MODEL-FREE SPEED CONTROLLER

A. ULTRA-LOCAL MODEL

The principle of super local model control is local modeling and updating it in real-time from input knowledge and output performance. In general, nonlinear systems can be expressed by unknown differential equations:

$$H(ty(t)y(t)^1 \cdots y(t)^n u(t)u(t)^1 \cdots u(t)^m) = 0 \tag{6}$$

where, u, y are the control input and control output in the system, respectively; H is a fully smooth function of its parameters. To obtain the desired output, an ultra-local model is defined to estimate parameters by measuring inputs and outputs. In a relatively short time, it is possible to use hyper-local models to represent purely digital models of systems.

$$y^{\varepsilon} = G + au \tag{7}$$

in the above equation, ε is the derivative of the system, $\varepsilon \geq 1$; a is a non-physical constant parameter, and G is an ultra-local model parameter, including all structural parameters, such as uncertainty, disturbance, and its derivatives.

In the system modeling accuracy of formula (7), the MFC method is further improved by using a first-order ultra-local model to design: $\varepsilon = 1$:

$$\dot{y} = G_{est} + au \tag{8}$$

according to formula (8), u can be obtained as:

$$u = \frac{-G_{est} + \dot{y}^* + \lambda}{a} \tag{9}$$

where, G_{est} is an estimate of G; y^* is the expected output value; λ is given by the proportional controller.

It can be obtained from formula (9):

$$u = \frac{-G_{est} + \dot{y}^* + K_p e}{a} \tag{10}$$

where, e is the error, namely $e = y^* - y$; K_p is the proportional controller coefficient.

Based on the equations of classical algorithms mentioned in reference 18:

$$L_{p_1}(s)J_1 + L_{p_2}(s)J_2 = \frac{G_{est}}{s} + I(s) \tag{11}$$

in the above formula, $L_{p_1}, L_{p_2} \in R\left[s,\ s-1\right]$are Laurent polynomials, $I \in R[s]$is a polynomial associated with the initial conditions.

With the formula (8), formula (11) becomes

$$sY = \frac{G_{est}}{s} + aU + y_0 \tag{12}$$

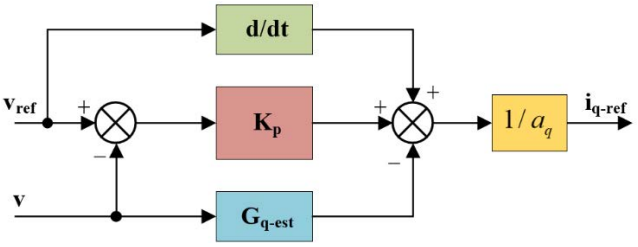

FIGURE 2. Block diagram of PMSLM model-free speed control system.

in the above formula, y_0 is the initial condition corresponding to the time interval $\left[t - L_e,\ t\right]$.

Get rid of y_0 by multiplying both sides by d/ds:

$$y + s\frac{dy}{ds} = -\frac{G_{est}}{s^2} + a\frac{du}{ds} \tag{13}$$

Multiplying both sides by s^{-2} for smoothing the noise yields in time domain yields, and the formula for G_{est} can be obtained by the parameter identification technique in reference 18, as follows

$$G_{est} = -\frac{6}{L_e^3}\int_{t-L_e}^{t} ((L_e - 2\sigma)y(\sigma) + a\sigma(L_e - \sigma)u(\sigma))d\sigma \tag{14}$$

where L_e is quite small.

B. PMSLM MODEL-FREE SPEED CONTROL

Based on the mathematical model of the PMSLM control system, the PMSLM super-local model is established according to formula (8):

$$\frac{dv}{dt} = G_q + a_q i_q \tag{15}$$

where, a_q is the stator current coefficient of q-axis; G_q represents known parts of PMSLM control system, uncertain parameters, and unknown parts such as multiple system interference.

$$G_{q-est} = -\frac{6}{T_F^3}\int_0^{T_F} ((T_F - 2\sigma)v(\sigma) + a_q\sigma(T_F - \sigma)i_q(\sigma))d\sigma \tag{16}$$

where, T_F is the sampling period of the system; G_{q-est} is an estimate of G_{est}.

The system block diagram of the PMSLM model-free speed controller is shown in Figure 2. The relationship between the modules in Figure 2 is as follows:

For the surface-mounted PMSLM, the stator reference value of the linear motor in the d-axis is set to 0, and the complex trapezoidal formula is used to calculate the approximate value of the definite integral. Meanwhile, formula (16) is used to estimate G_{q-est} online, which can be obtained:

$$G_{q-est} = -\frac{3}{m_F^3 T_s}\sum_{n=1}^{m_F}\{(m_F - 2(n-1))v[n-1] + a_q(n-1)\cdot T_s(m_F - (n-1))i_{q-ref}[n-1] + (m_F - 2n)v[n]$$

$$+a_q nT_s(m_F - n)i_{q-ref}\ [n]\} \tag{17}$$

where, $i_{q-ref}[n]$ and $v[n]$ are discrete sampling values of the system; m_F indicates the sampling step of the system. The larger m_F, the greater the amount of computation of the system; The smaller the m_F, the lower the accuracy of the system.

According to formula (10), the model-free controller of the PMSLM control system is designed, and the estimated value of the q-axis current is:

$$i_{q-est} = \frac{-G_{est} + dv/dt + K_{pc}(v_{ref} - v)}{a_q} \tag{18}$$

where, i_{q-est} is the estimated current of the q-axis; v_{ref} and v are the reference values and actual values of speed respectively. K_{pc} is the proportional controller coefficient.

IV. DESIGN AND STABILITY ANALYSIS OF MRAS

SMO is a special nonlinear control system, which has a switching characteristic that the structure changes at any time. The key of SMO is the selection of sliding mode surface function and sliding mode gain. SMO is a robust control method because it does not require the high accuracy of the system model and is insensitive to parameter changes and external disturbances. However, system buffeting is often caused by its inherent characteristics.

In this design, the MRAS observer is introduced to eliminate the dependence of the PMSLM control system on sensors, and further extract the speed information of PMSLM with high accuracy. MRAS observer can be divided into three parts: reference model, adjustable model, and reference adaptive control law. Using the difference between the output of the reference model and the adjustable model, an appropriate adaptive rate is designed to adjust the parameters of the adjustable model in real-time, to realize the process of the adjustable model following the reference model, with better tracking accuracy and smaller buffeting amplitude. At the same time, compared with SMO, MRAS has less computation.

To ensure the stability of MRAS designed in this paper, Popov hyperstability theory and Lyapunov stability theory are used to analyze the stability of MRAS.

For the PMSLM control system, the equation of stator current can be obtained by rewriting formula (1):

$$\begin{cases} \frac{d}{dt}i_d = -\frac{R}{L}i_d + \omega_c \cdot i_q + \frac{1}{L}u_d \\ \frac{d}{dt}i_q = -\frac{R}{L}i_q - \omega_c \cdot (i_d + \frac{\psi_f}{L}) + \frac{1}{L}u_q \end{cases} \tag{19}$$

by transforming formula (19):

$$\begin{cases} \frac{d}{dt}(i_d + \frac{\psi_f}{L}) = -\frac{R}{L} \cdot (i_d + \frac{\psi_f}{L}) + \omega_c \cdot i_q \\ \qquad +\frac{1}{L} \cdot (u_d + \frac{R}{L}\psi_f) \\ \frac{d}{dt}i_q = -\frac{R}{L}i_q - \omega_c \cdot (i_d + \frac{\psi_f}{L}) + \frac{1}{L}u_q \end{cases} \tag{20}$$

as defined below:

$$\begin{cases} i'_d = i_d + \frac{\psi_f}{L} \\ i'_q = i_q \\ u'_d = u_d + \frac{R}{L}\psi_f \\ u'_q = u_q \end{cases} \tag{21}$$

substitute formula (21) into formula (20):

$$\begin{cases} \frac{d}{dt}i'_d = -\frac{R}{L}i'_d + \omega_c \cdot i'_q + \frac{1}{L}u'_d \\ \frac{d}{dt}i'_q = -\frac{R}{L}i'_q - \omega_c \cdot i'_d + \frac{1}{L}u'_q \end{cases} \tag{22}$$

rewrite formula (22) into the state-space equation:

$$\frac{d}{dt}\begin{bmatrix} i'_d \\ i'_q \end{bmatrix} = \begin{bmatrix} -\frac{R}{L} & \omega_c \\ -\omega_c & -\frac{R}{L} \end{bmatrix}\begin{bmatrix} i'_d \\ i'_q \end{bmatrix} + \begin{bmatrix} \frac{1}{L} & 0 \\ 0 & \frac{1}{L} \end{bmatrix}\begin{bmatrix} u'_d \\ u'_q \end{bmatrix} \tag{23}$$

The above formula contains the mover speed information of the linear motor and can be used as an adjustable model, and the reference model is the PMSLM model.

Rewrite formula (22) to the form of estimated value:

$$\begin{cases} \frac{d}{dt}\hat{i}'_d = -\frac{R}{L}\hat{i}'_d + \hat{\omega}_c \cdot \hat{i}'_q + \frac{1}{L}u'_d \\ \frac{d}{dt}\hat{i}'_q = -\frac{R}{L}\hat{i}'_q - \hat{\omega}_c \cdot \hat{i}'_d + \frac{1}{L}u'_q \end{cases} \tag{24}$$

the generalized error $e = \begin{bmatrix} e_d & e_q \end{bmatrix}^T$ is defined as follows:

$$\begin{bmatrix} e_d \\ e_q \end{bmatrix} = \begin{bmatrix} i'_d \\ i'_q \end{bmatrix} - \begin{bmatrix} \hat{i}'_d \\ \hat{i}'_q \end{bmatrix} \tag{25}$$

make a difference between formula (22) and formula (24) and substitute it into formula (25):

$$\frac{d}{dt}\begin{bmatrix} e_d \\ e_q \end{bmatrix} = \begin{bmatrix} -\frac{R}{L} & \omega_c \\ -\omega_c & -\frac{R}{L} \end{bmatrix}\begin{bmatrix} e_d \\ e_q \end{bmatrix} - D(\omega_c - \widehat{\omega}_c)\begin{bmatrix} \hat{i}'_d \\ \hat{i}'_q \end{bmatrix} \tag{26}$$

in the above formula,$D = \begin{bmatrix} 0 & -1 \\ 1 & 0 \end{bmatrix}$.

Rewrite formula (26):

$$\frac{d}{dt}\begin{bmatrix} e_d \\ e_q \end{bmatrix} = E\begin{bmatrix} e_d \\ e_q \end{bmatrix} - \omega \tag{27}$$

in the above formula, $E = \begin{bmatrix} -\frac{R}{L} & \omega_c \\ -\omega_c & -\frac{R}{L} \end{bmatrix}, \omega = D\left(\omega_c - \hat{\omega}_c\right)\hat{i}_d$.

According to the Popov hyperstability theory, if the control system operates stably, it needs to meet the Popov inequality of:

$$\eta\left(0, t_{f1}\right) = \int_0^{t_{f1}} V^{\mathrm{T}} W dt \geq -\gamma_0^2 \left(t_{f1} \geq 0, 0 \leq \gamma_0 \leq \infty\right) \tag{28}$$

in the above formula, V refers to the system input to be proved; W refers to the system output to be proved stable.

The reverse evaluation of formula (28) shows that the reference adaptive law is:

$$\hat{\omega}_c = \int_0^{t_{f1}} K_{if}\left(i'_d\hat{i}'_q - \hat{i}'_d i'_q\right)d\tau + K_{pf}\left(i'_d\hat{i}'_q - \hat{i}'_d i'_q\right) \tag{29}$$

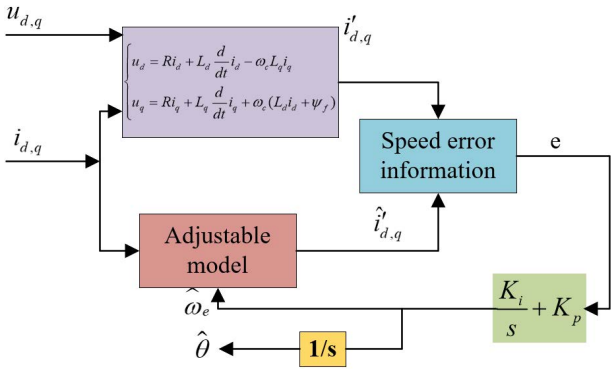

FIGURE 3. Block diagram of model reference adaptive system.

by integrating formula (29), the estimated position of PMSLM is:

$$\hat{\theta} = \int \hat{\omega}_c d\tau \tag{30}$$

The block diagram of the model reference adaptive system is shown in Figure 3.

The global stability of MRAS observer is further proved by the Lyapunov stability theory. The proof process is as follows:

Convert formula (19) to the following formula:

$$\dot{X} = AX + Br + Cl \tag{31}$$

where:

$$X = \begin{bmatrix} i_d \\ i_q \end{bmatrix}, A = \begin{bmatrix} -\frac{R}{L} & \omega_c \\ \omega_c & -\frac{R}{L} \end{bmatrix}, B = \frac{1}{L},$$
$$r = \begin{bmatrix} u_d \\ u_q \end{bmatrix}, C = -\frac{\psi_f}{L}, l = \begin{bmatrix} 0 \\ \omega_c \end{bmatrix}$$

The variable model can also be described as

$$\dot{\hat{X}} = \hat{A}\hat{X} + \hat{\boldsymbol{B}}\hat{r} + \hat{\boldsymbol{C}}\hat{\boldsymbol{l}} \tag{32}$$

where:

$$\hat{X} = \begin{bmatrix} \hat{i}_d \\ \hat{i}_q \end{bmatrix}, \hat{A} = \begin{bmatrix} -\frac{\hat{R}}{\hat{L}} & \omega_c \\ \omega_c & -\frac{\hat{R}}{\hat{L}} \end{bmatrix}, \hat{B} = \frac{1}{\hat{L}},$$
$$r = \begin{bmatrix} u_d \\ u_q \end{bmatrix}, \hat{C} = -\frac{\hat{\psi}_f}{\hat{L}}, \hat{l} = \begin{bmatrix} 0 \\ \omega_c \end{bmatrix} = l$$

The errors can be expressed as

$$e_L = X - \hat{X} = \begin{bmatrix} e_{L_1} \\ e_{L_2} \end{bmatrix} \tag{33}$$

The entire MRAS observer system is transformed into an error state equation as:

$$\begin{aligned} \dot{e}_L &= AX + Br + Cl - \hat{A}\hat{X} - \hat{B}r - \hat{C}\hat{l} \\ &= AX - A\hat{X} + A\hat{X} - \hat{A}\hat{X} + Br - \hat{B}r + Cl - \hat{C}\hat{l} \\ &= Ae_L + \left(A - \hat{A}\right)\hat{X} + (B - \hat{B})r + h \end{aligned} \tag{34}$$

as defined below:

$$\begin{aligned} &b = B - \hat{B} = \left(\frac{1}{L} - \frac{1}{\hat{L}}\right), \alpha = \left(\frac{\hat{R}}{\hat{L}} - \frac{R}{L}\right), \\ &h = (C - \hat{C})l, g = C - \hat{C}, \delta^T = \begin{bmatrix} \alpha & b & g \end{bmatrix}, \\ &s_L = \begin{bmatrix} \hat{X} & r & l \end{bmatrix}^T \end{aligned} \tag{35}$$

Convert formula (34) to:

$$\dot{e}_L = Ae_L + \delta^T s_L \tag{36}$$

A Lyapunov function is designed as below, which is in the usual positive definite form.

$$V_L\left(X, t_L\right) = \frac{e_L^T P e_L + \delta^T Q \delta}{2} \tag{37}$$

where:

$$P = \begin{bmatrix} 1 & 0 \\ 0 & 1 \end{bmatrix} = P^T, Q = \begin{bmatrix} 1 & 0 & 0 \\ 0 & 1 & 0 \\ 0 & 0 & 1 \end{bmatrix} = Q^T$$

$V_L\left(X, t_L\right)$ is positive definite. The Lyapunov second theorem on stability is employed here to ensure the global asymptotic stability of the system, and $e_L = \delta^T = 0$ is set as the stable equilibrium point. The Lyapunov stability theorem is shown as follows:

1. $V_L\left(X, t_L\right)$ is positive definite
2. $\dot{V}_L\left(X, t_L\right)$ is negative definite
3. $V_L\left(X, t_L\right)$ is infinite when $|X| \to \infty$

It is obvious that requires 1 and 3 are achieved, and require 2 is discussed as follows:

$$\begin{aligned} \dot{V}_L(X,t_L) &= \frac{1}{2}\left(\dot{e}_L^T P e_L + e_L^T P \dot{e}_L + \dot{\delta}^T Q \delta + \delta^T Q \dot{\delta}\right) \\ \dot{e}_L^T P e_L &= e_L^T A^T P e_L + s_L^T \delta P e_L \\ e_L^T P \dot{e}_L &= e_L^T P(A e_L) + e_L^T P(\delta^T s_L) \\ \dot{\delta}^T Q \delta + \delta^T Q \dot{\delta} &= 2(\alpha\dot{\alpha} + b\dot{b} + g\dot{g}) \\ &\Rightarrow \dot{V}_L(X,t_L) = \frac{1}{2} e_L^T (PA + A^T P) e_L \\ &+ \frac{1}{2}(s_L^T \delta P e_L + e_L^T P(\delta^T s_L)) \\ &+ \alpha\dot{\alpha} + b\dot{b} + g\dot{g} \end{aligned} \tag{38}$$

where:

$$PA + A^T P = -Z = \begin{bmatrix} -2\frac{R}{L} & 0 \\ 0 & -2\frac{R}{L} \end{bmatrix}$$
$$\begin{aligned} &\frac{1}{2}(s_L^T \delta P e_L + e_L^T P(\delta^T s_L)) \\ &= \alpha\hat{i}_d(i_d - \hat{i}_d) + \alpha\hat{i}_q(i_q - \hat{i}_q) + bu_d(i_d - \hat{i}_d) \\ &+ (bu_q + \omega_c g)(i_q - \hat{i}_q) \end{aligned}$$

where $(R/L) > 0$, it is obvious that $e_L^T(PA + A^T P)e_L/2$ is negative definite.

Therefore,

$$\begin{aligned} \dot{V}_L(X,t_L) &= \frac{1}{2} e_L^T (PA + A^T P) e_L + \alpha\hat{i}_d(i_d - \hat{i}_d) \\ &+ \alpha\hat{i}_q(i_q - \hat{i}_q) + bu_d(i_d - \hat{i}_d) \end{aligned}$$

TABLE 1. PMSLM main parameters.

Parameter	Value
Stator resistance Rs	4.0Ω
D-axis inductance L	8.2 mH
Q-axis inductance L	8.2 mH
Moment mass m	1.425kg
Viscous friction coefficient B	44N·m·s
Pole distance τ	0.016m

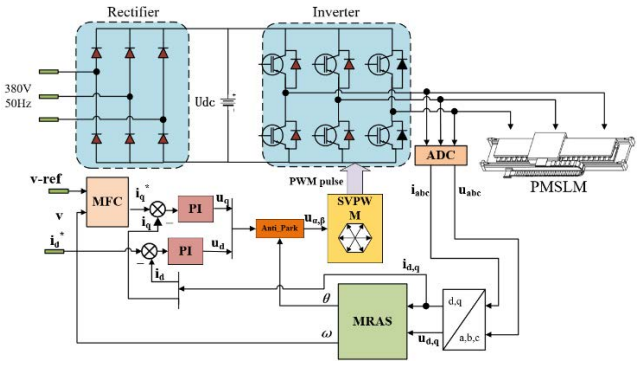

FIGURE 4. PMSLM control system block diagram.

$$
\begin{aligned}
&+(bu_q+\omega_c g)(i_q-\hat{i}_q)+\alpha\dot{\alpha}+b\dot{b}+g\dot{g}\\
&=\alpha(\hat{i}_d(i_d-\hat{i}_d)+\hat{i}_q(i_q-\hat{i}_q)+\dot{\alpha})+b(u_d(i_d-\hat{i}_d)\\
&\quad+u_q(i_q-\hat{i}_q)+\dot{b})+g\left[\omega_c(i_q-\hat{i}_q)+\dot{g}\right]\\
&\quad+\frac{1}{2}e_L^T(PA+A^TP)e_L \qquad (39)
\end{aligned}
$$

Then, it is easy to obtain the adaptive law from the formula (39).

Let,

$$
\begin{aligned}
\alpha(\hat{i}_d(i_d-\hat{i}_d)+\hat{i}_q(i_q-\hat{i}_q)+\dot{\alpha})&=0\\
b(u_d(i_d-\hat{i}_d)+u_q(i_q-\hat{i}_q)+\dot{b})&=0\\
\omega_c(i_q-\hat{i}_q)+\dot{g}&=0 \qquad (40)
\end{aligned}
$$

Then, it is obvious that $\dot{V}_L\left(X,\ t_L\right)$ is negative definite and require 2 is satisfied. The whole system is therefore globally asymptotically stable to converge to the equilibrium point.

V. SIMULATION ANALYSIS AND EXPERIMENTAL VERIFICATION

A. SYSTEM SIMULATION

The block diagram of this design and establishment system is shown in Figure 4, and according to the motor drive parameters indicated in Table 1, a simulation model is established in the simulation platform for simulation analysis, and the motor speed and thrust under the conditions of speed regulation and variable load are compared. The waveforms of the MFC and the PI controller and the SMC controller are further analyzed to verify the feasibility and effectiveness of the sensorless vector control method of the PMSLM based on

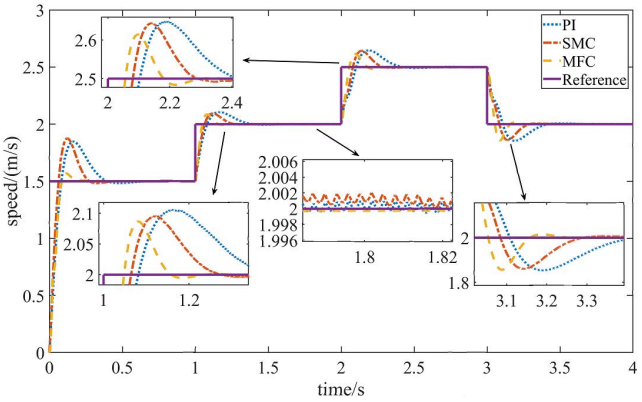

FIGURE 5. Comparison of variable speed motion.

the MFC proposed in this paper. Then an adaptive observer is added based on the MFC based on the speed loop, and the observation performance of the designed adaptive observer and SMO on the velocity of the control system is compared. The sampling time of the system is μs.

The controller parameters selected in this design are selected through the empirical tuning method. In the process of simulation comparison, the parameters of the PI control system speed loop are: $K_{p1} = 1.2$, $K_{i1} = 10$. The sliding surface defined by the speed loop controller of the SMC control system is $s_{mc} = c_{mc} \cdot x_{mc1} + x_{mc2}(x_{mc1}, x_{mc2}$ is the state variable). The adopted approach rate is $\dot{s}_{mc} = -\phi \cdot sgn(s_{mc}) - q_{mc} \cdot s_{mc}$, the parameter of the controller is: $c_{mc} = 15$, $\phi = 150$, $q_{mc} = 300$. Keep the parameters of the current loop controller the same. The parameters of the MFC are:$m_F = 30$, $K_{pc} = 7000$, $a_q = 350$. The parameters of the MRAS are: $K_{pf} = 30$, $K_{if} = 500$.

Set the motor load as 50N, give the variable speed motion command of the PMSLM control system, and the speed change is 1.5m/s→2m/s→2.5m/s→2m/s, which can not only observe the specified medium and high speed running speed waveform of the control system but also observe the dynamic response of the motor speed in the case of rising and falling. Figure 5 shows the operating speed waveform of the linear motor under the application of model-free speed controller and PI controller and SMC controller.

As can be seen from Figure 5, compared with the PI controller and SMC controller, the MFC controller designed in this paper not only has small overshoot, but also greatly shortens the adjustment time after speed regulation, no matter whether the motor is accelerating or decelerating. Compared with the PI controller and SMC controller, the MFC controller proposed in this paper has less jitter and stronger stability in the high-speed operation stage of 2.5m/s. Through the simulation analysis of variable speed motion, it is proved that the model-free speed control system proposed in this paper has superior dynamic control performance.

Figure 6 shows the thrust change waveform of the three systems when the operating speed changes. It can be seen from Figure 6 that when the operating speed changes, the

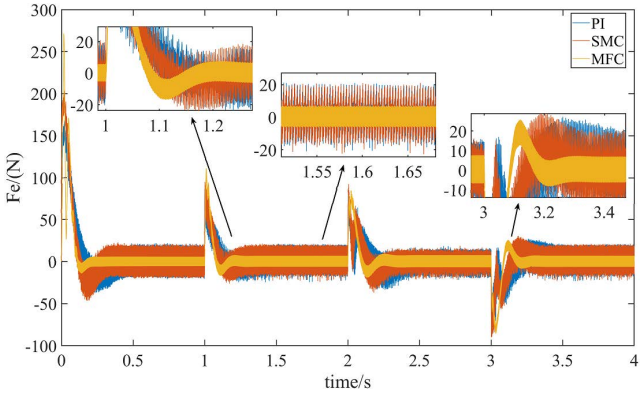

FIGURE 6. Thrust comparison in variable speed motion.

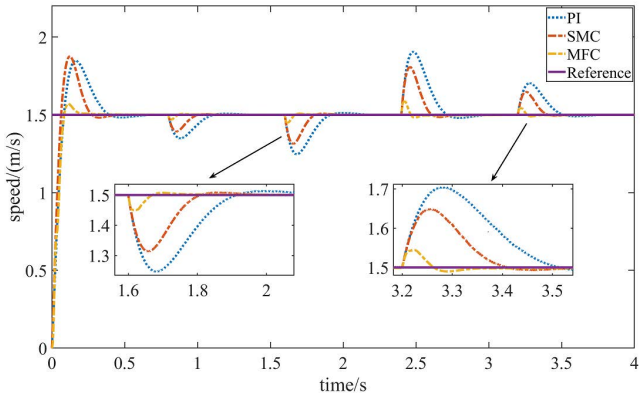

FIGURE 7. Speed change under variable load.

thrust in the MFC controller changes rapidly, and the thrust is nearly stable within 0.1s. MFC controller shows the same dynamic response performance when the running speed drops suddenly. When the speed increases or decreases, the PI controller needs about 0.25s to approach the steady-state of thrust. The SMC controller needs about 0.2s to make the thrust close to a steady-state.

In Figure 6, the thrust waveform jitter of the MFC controller is small and relatively stable, and the jitter amplitude is about 10N. The thrust waveform jitter amplitude of the PI controller and SMC controller is similar, and the jitter amplitude is about 35N, which is 3.5 times that of the MPC system.

The given speed of the PMSLM system is 1.5m/s. during the operation of the system, the load is changed in the control system, and the load change is 30N→50N→80N→40N. It is used to compare the speed and thrust changes of the MFC controller and PI controller and SMC controller under the condition of sudden increase and sudden drop of load, to analyze the anti-disturbance performance of the control system.

In Figure 7, when the additional load is 50N, the speed change of the MFC system is about 0.05m/s, and the adjustment time is about 0.09s. The speed change of the PI system is about 0.28m/s, which is about 6 times that of the MFC system. The adjustment time of the PI system is about 0.3s, about 3 times that of the MFC system. The speed change of the SMC system is about 0.18m/s, which is about 4 times that of the MFC system. The adjustment time of the SMC system is about 0.2s, about twice that of the MFC system.

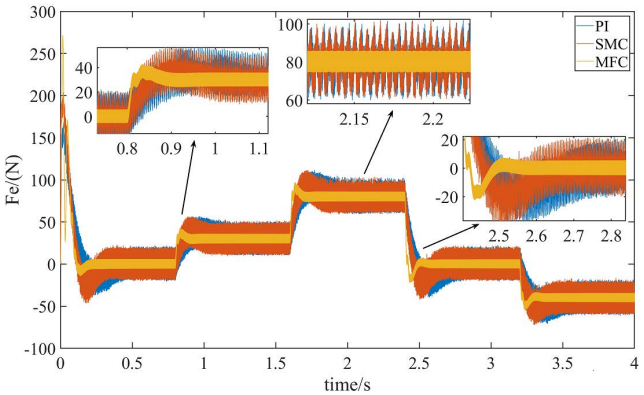

FIGURE 8. Thrust change under variable load.

When the additional load is 80N, the speed change of the MFC system is about 0.1m/s, and the adjustment time is about 0.12s. The speed change of the PI system is about 0.4m/s, which is 4 times that of the MFC system. The adjustment time of the PI system is about 0.35s, about 3 times that of the MFC system. The speed change of the SMC system is about 0.3m/s, which is three times that of the MFC system. The adjustment time of the SMC system is about 0.23s, about twice that of the MFC system.

It can be seen from Figure 7 that the speed fluctuation and adjustment time of the MFC system are smaller than those of the PI system and SMC system when the load increases or decreases suddenly.

Figure 8 shows the thrust change waveform of the three systems when the additional load value changes. It can be seen from figure 8 that when the load increases suddenly, the thrust in the MFC system changes rapidly, and the thrust is close to the value of the additional load only within 0.06s. When the load drops suddenly, the control system shows the same dynamic response performance. When the load of the PI system suddenly increases or decreases, the PI system needs about 0.18s to change the thrust to a value close to the increased load. When the SMC system load suddenly increases or decreases, the SMC system needs about 0.12s to change the thrust to a value close to the increased load.

In Figure 8, the thrust waveform jitter of the MFC system is small and relatively stable, and the jitter amplitude is about 10N. The thrust waveform jitter amplitude of the PI system and SMC system is similar, and the jitter amplitude is about 35N, which is 3.5 times that of the MFC system.

Add random load as shown in Figure 9 to the system and observe the operation of the system to analyze the anti-disturbance ability of the system. Figure 10 shows the comparison of the running speeds of the three control systems with random loads when the system speed is given at 1.5m/s.

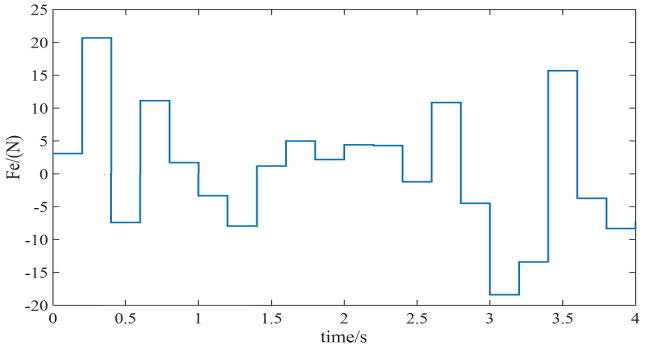

FIGURE 9. Random load added to the control system.

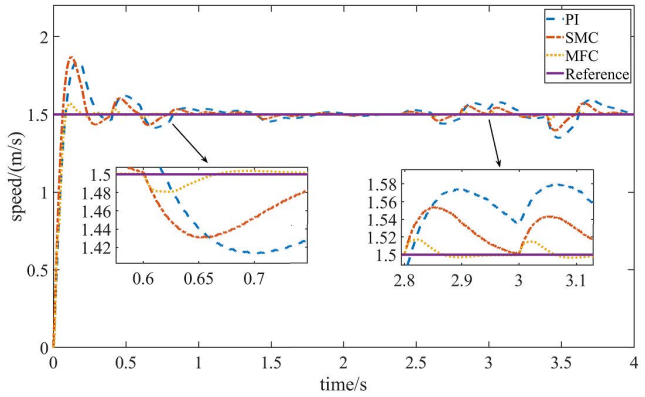

FIGURE 10. Comparison of running speed under random load.

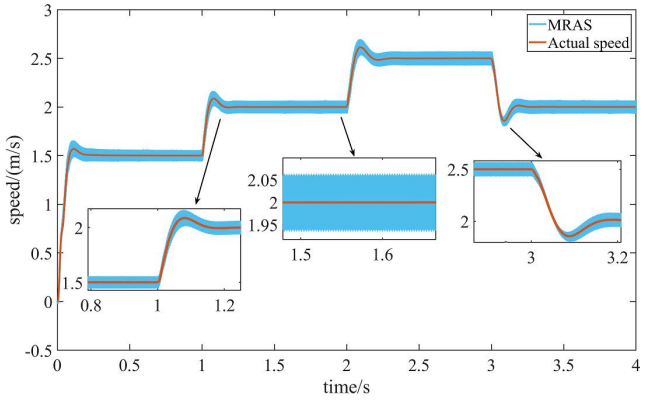

FIGURE 11. Comparison between estimated speed and actual speed of the MRAS observer.

Among the three control strategies, the MFC system is better than the PI system and SMC system. When the speed reaches the given speed, the speed fluctuation of the proposed MFC system is minimum and more stable.

After verifying that the proposed MFC has better control performance than the PI controller and the SMC controller, the MRAS observer designed in this paper is added to the MFC system, which is compared with the SMO for variable speed operation. Figures 11 and 12 show the comparison between the estimated speed and the actual speed of the control system after adding the MRAS observer and the SMO.

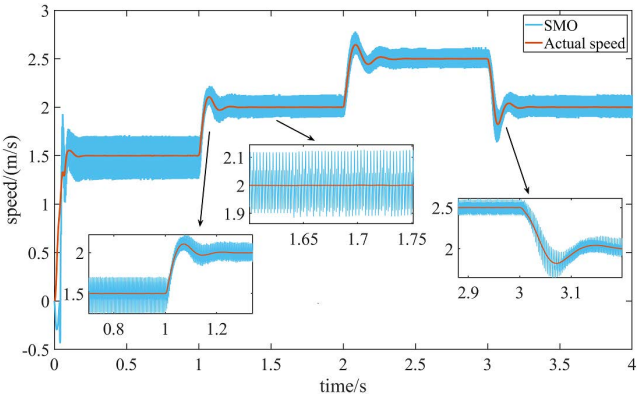

FIGURE 12. Comparison between estimated speed and actual speed of the SMO system.

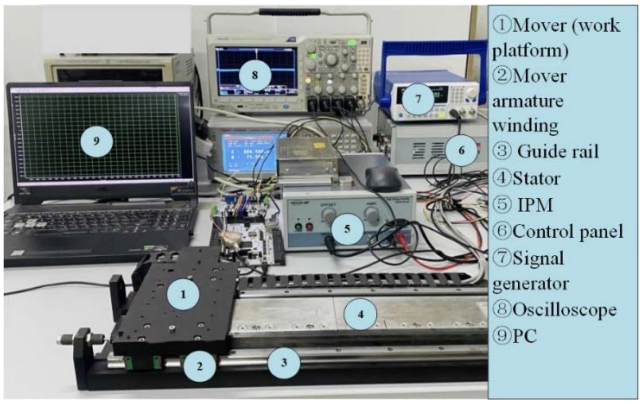

FIGURE 13. Experimental platform diagram.

Regardless of the sudden increase or decrease of speed, the adjustment time and fluctuation value of the MRAS observer in the overall speed waveform are much smaller than that of the SMO, and the MRAS observer has stronger tracking performance and stability than the SMO. In the whole running time, the fluctuation value of the MRAS observer is always stable at 0.1m/s, and the waveform is smooth. The minimum fluctuation value of the SMO is 0.2m/s, and the adjustment time is long when the speed changes.

B. EXPERIMENTAL VERIFICATION

To verify the feasibility and effectiveness of the sensorless vector control method of PMSLM based on model-free speed control proposed in this paper, hardware in the loop simulation platform is built in the laboratory for verification, and a TMS320F28335 digital processing chip is used to realize the control. The experimental platform is shown in Figure 13. This experiment compares and analyzes the speed waveform under variable load during motor operation, the speed adjustment time and fluctuation value after increasing or decreasing load, and the tracking performance of the observer used. The motor parameters in the experiment are consistent with the simulation. The sampling time of the system in the experiment is set to 500 μs.

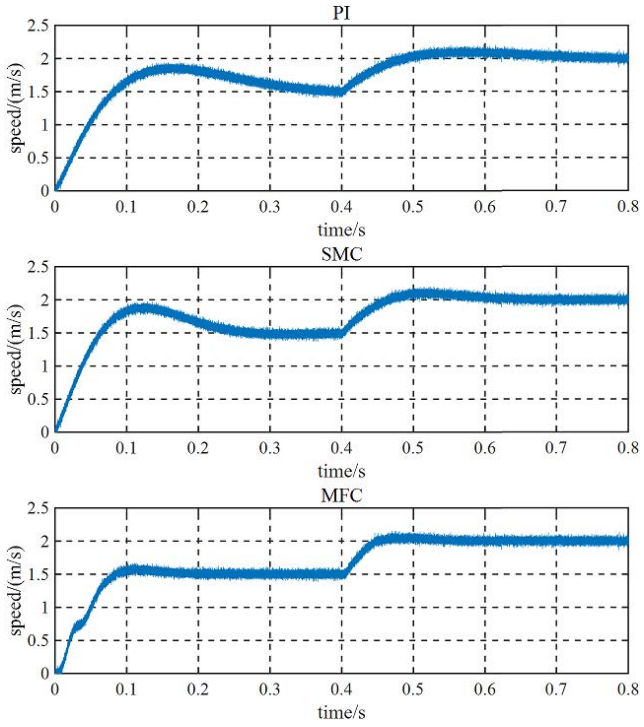

FIGURE 14. Comparison of speed waveforms of three controllers under speed variation.

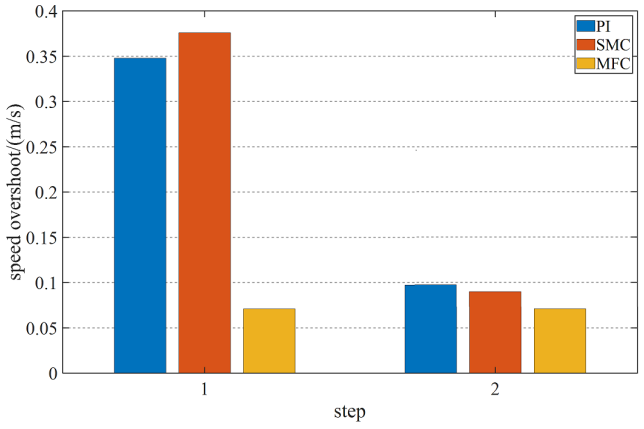

FIGURE 15. Comparison of speed overshoot of three controllers under speed variation.

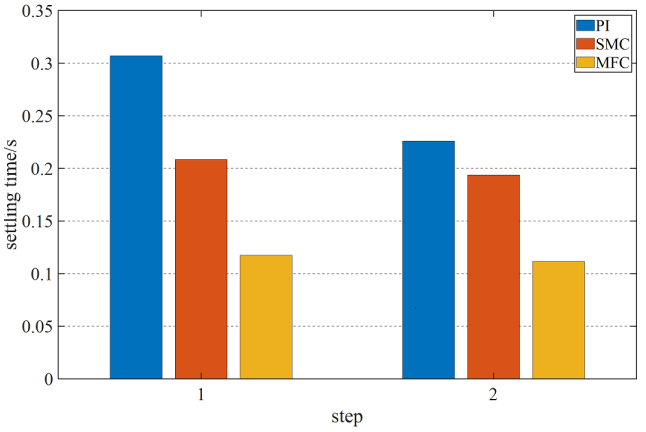

FIGURE 16. Comparison of settling time of three controllers under speed variation.

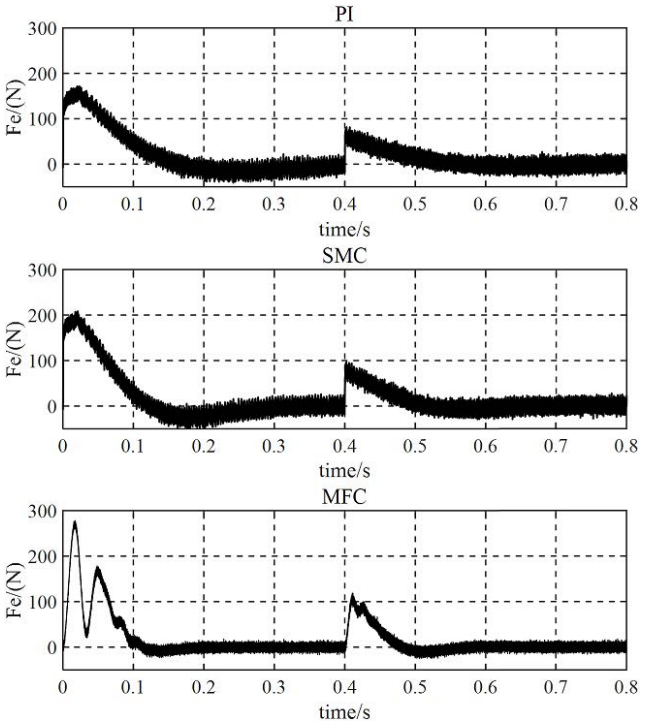

FIGURE 17. Thrust comparison of three controllers under speed variation.

Because the actual environment in the experiment is different from the ideal environment in the simulation. To make the PMSLM run more stably, the given speed of the control system is 1.5m/s under the condition of light load, and the given speed is increased to 2m/s at 0.4s. Figure 14 shows the speed waveform of the three control systems. Figure 15 shows the speed overshoot of the three control systems. Figure 16 shows the setting time of the three control systems.

It can be seen from Figure 15 and Figure 16 that the overshoot of the PI system in the two motion stages is 0.35m/s and 0.1m/s respectively, and the adjustment time is 0.3s and 0.23s respectively. The overshoot of the SMC system in the two motion stages is 0.37m/s and 0.09m/s respectively, and the adjustment time is 0.2s and 0.19s respectively. The overshoot of the MFC system in two motion stages is 0.07m/s and 0.08m/s respectively, and the adjustment time is 0.113s and 0.111s respectively. It can be seen from Figure 15 and Figure 16 that the MFC system in this paper has a smaller overshoot and regulation time than the PI control system and SMC system, which reflects that the MFC system has the strong anti-interference ability and high control performance.

Figure 17 shows the thrust waveform changes of the current MFC system, PI system, and SMC system after the operating speed changes. After the operating speed changes, the thrust of the MFC system quickly recovers to be stable.

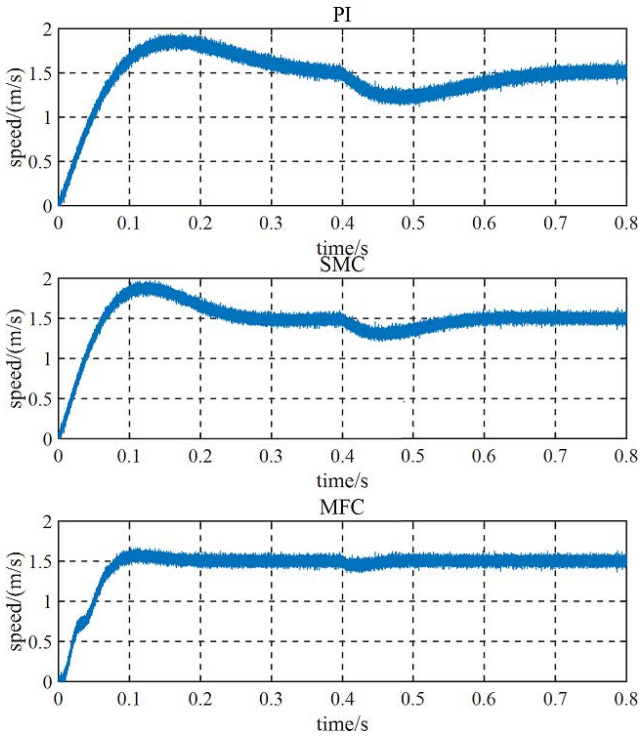

FIGURE 18. Speed waveform comparison of three controllers under load change.

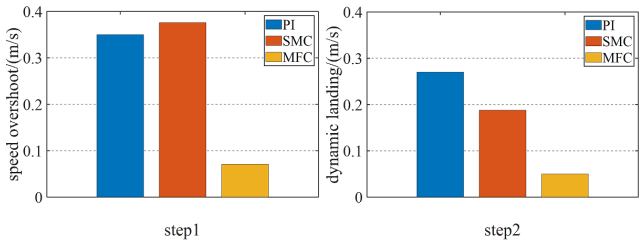

FIGURE 19. Comparison of speed overshoot and dynamic landing of three controllers under load change.

It takes a long time for the PI system and SMC system to restore the thrust smoothly. At the same time, compared with the PI system and SMC system, the MFC system has a more stable thrust waveform, less jitter, and faster response speed.

Set the system speed to 1.5m/s and add a 50N load at 0.4s. Figure 18 shows the speed waveform of the three control systems. Figure 19 shows the speed overshoot of the three control systems. Figure 20 shows the setting time of the three control systems.

It can be seen from Figure 19 and Figure 20 that the overshoot and the dynamic landing of PI system in the two motion stages are 0.35m/s and 0.27m/s respectively, and the adjustment time is 0.31s and 0.30s respectively. The overshoot and the dynamic landing of the SMC system in two motion stages are 0.37m/s and 0.19m/s respectively, and the adjustment time is 0.21s and 0.20s respectively. The overshoot and the dynamic landing of the MFC system in two motion stages are

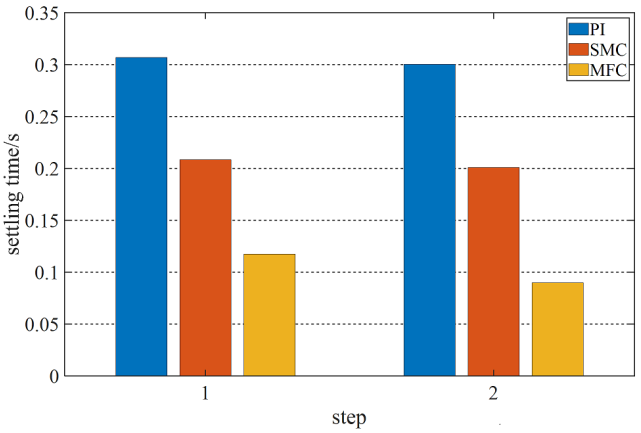

FIGURE 20. Comparison of settling time of three controllers under load change.

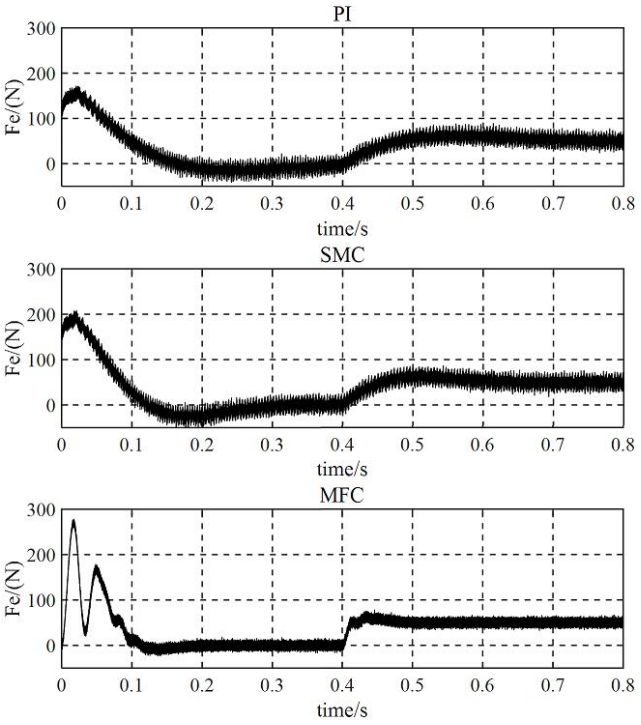

FIGURE 21. Thrust comparison of three controllers under load change.

0.07m/s and 0.05m/s respectively, and the adjustment time is 0.12s and 0.08s respectively.

It can be seen from Figure 19 and Figure 20 that the MFC system in this paper has a smaller overshoot and dynamic landing, and regulation time than the PI control system and SMC system, which reflects that the MFC system has strong control performance

Figure 21 shows the thrust waveform change of the current MFC system, PI system, and SMC system after load change. After the load changes, the thrust of the MFC system quickly returns to a stable state. It takes a long time for the PI system and SMC system to recover thrust smoothly. Compared with

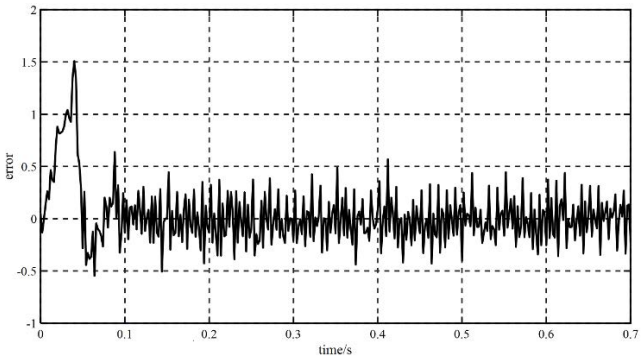

FIGURE 22. Speed error of the SMO.

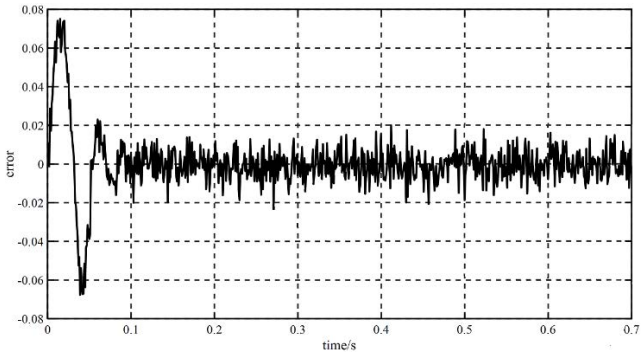

FIGURE 23. Speed error of the MRAS observer.

the PI system and SMC system, the MFC system has a more stable thrust waveform, less jitter, and faster response speed.

The MFC system is applied to the PMSLM, and the MRAS observer and the SMO are added. The given speed of the control system is 1.5m/s. Observe the difference between the estimated speed of the two systems and the speed detected by the mechanical sensor. It can be seen that the SMO in Figure 22 has greater chattering than the MRAS observer in Figure 23.

VI. CONCLUSION

Aiming at the problem that the traditional control methods in PMSLM are highly dependent on motor parameters, and to accurately estimate the mover speed required by the sensorless vector control system of PMSLM, the ultra-local model based MFC and an observer based on model reference adaptive system is proposed. For the controlled instability caused by the parameter uncertainty of traditional control methods in PMSLM, the designed MFC has strong robustness to the uncertainty of motor parameters, which can better improve the control performance of the system. Meanwhile, the designed MRAS simplifies the complexity and cost of the control system and improves the accuracy of PMSLM tracking speed. In the part of simulation and experiment, MFC is compared with PI controller and SMC controller. The comparison of overshoot and regulation time shows that MFC in this design has strong anti-interference and good control performance. At the same time, the velocity waveforms observed by MRAS and SMO are compared with those observed by mechanical sensors. The comparison of buffeting amplitude and error shows that MRAS has the advantages of fast convergence, high tracking accuracy, small buffeting, and good system stability. Through the simulation and experiment platform, it is fully verified that the control strategy can not only simplify the structure of the system but also improve the control performance of the control system in the sensorless state.

REFERENCES

[1] A. Boduroglu, M. Gulec, Y. Demir, E. Yolacan, and M. Aydin, "A new asymmetric planar V-shaped magnet arrangement for a linear PM synchronous motor," *IEEE Trans. Magn.*, vol. 55, no. 7, pp. 1–5, Jul. 2019.

[2] M. Li, J. Zhao, Y. Hu, and Z. Wang, "Active disturbance rejection position servo control of PMSLM based on reduced-order extended state observer," *Chin. J. Electr. Eng.*, vol. 6, no. 2, pp. 30–41, Jun. 2020.

[3] D. Xie, J. Yang, H. Cai, F. Xiong, B. Huang, and W. Wang, "Blended chaos control of permanent magnet linear synchronous motor," *IEEE Access*, vol. 7, pp. 61670–61678, 2019.

[4] C. Wen, J. Liu, W. Wang, J. Liu, Z. Zhao, and J. Liu, "Research on improved permanent magnet linear synchronous motor for direct-drive application," *IEEE Trans. Magn.*, vol. 55, no. 10, pp. 1–7, Oct. 2019.

[5] Q. Tan, M. Wang, and L. Li, "Analysis of a new flux switching permanent magnet linear motor," *IEEE Trans. Magn.*, vol. 57, no. 2, pp. 1–5, Feb. 2021.

[6] L. Zheng, W. Jinsong, A. Jinfeng, Z. Qingshan, and Z. Yiding, "Variable gain cross-coupling control system of dual-axis PM synchronous linear motor based on model predictive speed and current integrated controller," in *Proc. 13th Int. Symp. Linear Drives Ind. Appl. (LDIA)*, Jul. 2021, pp. 1–6.

[7] H. Dan, P. Zeng, W. Xiong, M. Wen, M. Su, and M. Rivera, "Model predictive control-based direct torque control for matrix converter-fed induction motor with reduced torque ripple," *CES Trans. Electr. Mach. Syst.*, vol. 5, no. 2, pp. 90–99, Jun. 2021.

[8] Z. Li, J. An, Q. Zhang, H. Liu, and H. Sun, "Design of PMSLM position controller based on model predictive control algorithm," *IEEE Access*, vol. 9, pp. 78835–78846, 2021.

[9] X. Li, Y. Wang, X. Guo, X. Cui, S. Zhang, and Y. Li, "An improved model-free current predictive control method for SPMSM drives," *IEEE Access*, vol. 9, pp. 134672–134681, 2021.

[10] D. Sun, X. Shao, and G. Feng, "A model-free cross-coupled control for position synchronization of multi-axis motions: Theory and experiments," *IEEE Trans. Control Syst. Technol.*, vol. 15, no. 2, pp. 306–314, Mar. 2007.

[11] S. A. Hashjin, A. Corne, S. Pang, K. Ait-Abderrahim, E.-H. Miliani, and B. Nahid-Mobarakeh, "Current sensorless control for WRSM using model-free adaptive control," *IEEE Trans. Transport. Electrific.*, vol. 7, no. 2, pp. 683–693, Jun. 2021.

[12] S.-Y. Chen, H.-H. Chiang, T.-S. Liu, and C.-H. Chang, "Precision motion control of permanent magnet linear synchronous motors using adaptive fuzzy fractional-order sliding-mode control," *IEEE/ASME Trans. Mechatronics*, vol. 24, no. 2, pp. 741–752, Apr. 2019.

[13] H. Niu, Z. Ma, Y. Han, G. Chen, Z. Liao, and G. Lin, "Model predictive control with common-mode voltage minimization for a three-level NPC inverter PMLSM drive system," in *Proc. 13th Int. Symp. Linear Drives Ind. Appl. (LDIA)*, Jul. 2021, pp. 1–5.

[14] J. Han, "From PID to active disturbance rejection control," *IEEE Trans. Ind. Electron.*, vol. 56, no. 3, pp. 900–906, Mar. 2009.

[15] D. Lu, G. Y. Zhao, Y. L. Qu, and D. L. Qi, "Permanent magnet synchronous motor control system based on no manual tuned active disturbance rejection control," *Trans. China Electrotech. Soc.*, vol. 28, no. 3, pp. 27–34, 2013.

[16] Z. Hou and S. Jin, "Data-driven model-free adaptive control for a class of MIMO nonlinear discrete-time systems," *IEEE Trans. Neural Netw.*, vol. 22, no. 12, pp. 2173–2188, Dec. 2011.

[17] R. M. Cao, H. X. Zhou, and Z. S. Hou, "Data-driven model-free adaptive precision control for linear servo system," *Control Theory Appl.*, vol. 29, pp. 310–316, Mar. 2012.

[18] M. Fliess and C. Join, "Model-free control," *Int. J. Control*, vol. 86, no. 12, pp. 2228–2252, 2013.
[19] J. Villagra, B. Vinagre, and I. Tejado, "Data-driven fractional PID control: Application to DC motors in flexible joints," *IFAC Proc.*, vol. 45, no. 3, pp. 709–714, 2012.
[20] M.-B. Radac, R.-C. Roman, R.-E. Precup, and E. M. Petriu, "Data-driven model-free control of twin rotor aerodynamic systems: Algorithms and experiments," in *Proc. IEEE Int. Symp. Intell. Control (ISIC)*, Oct. 2014, pp. 1889–1894.
[21] E. Zerdali, "A comparative study on adaptive EKF observers for state and parameter estimation of induction motor," *IEEE Trans. Energy Convers.*, vol. 35, no. 3, pp. 1443–1452, Sep. 2020.
[22] R. Nair and G. Narayanan, "Stator flux based model reference adaptive observers for sensorless vector control and direct voltage control of doubly-fed induction generator," *IEEE Trans. Ind. Appl.*, vol. 56, no. 4, pp. 3776–3789, Apr. 2020.
[23] Y.-C. Liu, S. Laghrouche, D. Depernet, A. Djerdir, and M. Cirrincione, "Disturbance-observer-based complementary sliding-mode speed control for PMSM drives: A super-twisting sliding-mode observer-based approach," *IEEE J. Emerg. Sel. Topics Power Electron.*, vol. 9, no. 5, pp. 5416–5428, Oct. 2021.
[24] J. Sun, G.-Z. Cao, S.-D. Huang, Y. Peng, J. He, and Q. Qian, "Sliding-mode-observer-based position estimation for sensorless control of the planar switched reluctance motor," *IEEE Access*, vol. 7, pp. 61034–61045, 2019.
[25] Y. Wang, Z. Lan, and G. Zhu, "Adaptive sliding mode observer based on phase locked loop in sensorless control of permanent magnet linear synchronous motor," in *Proc. 13th Int. Symp. Linear Drives Ind. Appl. (LDIA)*, Jul. 2021, pp. 1–6.
[26] R. Cao, N. Jiang, and M. Lu, "Sensorless control of linear flux-switching permanent magnet motor based on extended Kalman filter," *IEEE Trans. Ind. Electron.*, vol. 67, no. 7, pp. 5971–5979, Jul. 2020.
[27] J. Zhao, L. Wang, L. Xu, F. Dong, J. Song, and X. Yang, "Uniform demagnetization diagnosis for permanent-magnet synchronous linear motor using a sliding-mode velocity controller and an ALN-MRAS flux observer," *IEEE Trans. Ind. Electron.*, vol. 69, no. 1, pp. 890–899, Jan. 2022.
[28] E. Zerdali and E. C. Mengüç, "Novel complex-valued stator current-based MRAS estimators with different adaptation mechanisms," *IEEE Trans. Instrum. Meas.*, vol. 68, no. 10, pp. 3793–3795, Oct. 2019.

ZHENG LI (Member, IEEE) was born in Shijiazhuang, Hebei, China, in 1980. He received the B.Sc. degree in electrical engineering and the Ph.D. degree in power electronics and electric drive from the Hefei University of Technology, Hefei, China, in 2002 and 2007, respectively.

Since 2007, he has been a Lecturer, an Associate Professor, and a Professor with the School of Electrical Engineering, Hebei University of Science and Technology. From July 2013 to July 2014, he was a Visiting Scholar and a part-time Faculty Member at the College of Engineering, Wayne State University, USA. He is the author of more than 240 published papers. His current research interests include design, analysis, and control of novel motors and actuators, intelligent control, and power electronics.

Dr. Li is an active reviewer of the IEEE TRANSACTIONS ON INDUSTRIAL ELECTRONICS, IEEE TRANSACTIONS ON ENERGY CONVERSION, and IEEE TRANSACTIONS ON MAGNETICS, and *Electric Power Components and Systems*.

ZIHAO ZHANG was born in Henan, China, in 1999. He received the bachelor's degree in electrical engineering and automation from the Hebei University of Science and Technology, in 2021, where he is currently pursuing the master's degree.

His research interests include linear motor control algorithm and motor drive simulation.

SHENGDI FENG was born in Hebei, China in 1997. He received the bachelor's degree in electrical engineering and automation from the Hebei University of Science and Technology, in 2020, where he is currently pursuing the master's degree.

His research interest includes control system design of biaxial permanent magnet synchronous linear motor.

JINSONG WANG was born in Baoding, China, in 1998. He received the bachelor's degree in automation from the Hebei University of Science and Technology, in 2020, where he is currently pursuing the master's degree.

His research interests include special motor control and linear motor drive.

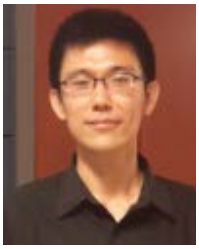

XIAOQIANG GUO (Senior Member, IEEE) received the B.S. and Ph.D. degrees in electrical engineering from Yanshan University, Qinhuangdao, China, in 2003 and 2009, respectively. He was a Postdoctoral Fellow at the Laboratory for Electrical Drive Applications and Research, Ryerson University, Toronto, ON, Canada. He is currently a Professor with the Department of Electrical Engineering, Yanshan University. He has authored or coauthored more than 80 technical articles and in addition to 11 patents. His current research interests include high-power converters and ac drives, electric vehicle charging station, and renewable energy power conversion systems. He is a Senior Member of the IEEE Power Electronics Society and the IEEE Industrial Electronics Society. He is an Associate Editor of the China Power Supply Society (CPSS) *Transactions on Power Electronics and Applications*, *Journal of Power Electronics*, and *IET Power Electronics*.

HEXU SUN (Senior Member, IEEE) received the Ph.D. degree in automation from Northeastern University, Shenyang, China, in 1993. He has been a Professor with the School of Control Science and Engineering, Hebei University of Technology, Tianjin, China, and the School of Electrical Engineering, Hebei University of Science and Technology, Shijiazhuang, China. He has authored five books and more than 130 journal and conference papers, and holds 13 U.S. patents and five computer software copyrights. His current research interests include robotics and complex engineering systems. He was a recipient of many prestigious national awards from China. He is the director in many societies and committees in China. He is currently the invited plenary speaker and a general co-chair of many international conferences.